11. SOLAR ARRAY PERFORMANCE

The solar arrays provided power for the satellite and payload in all but the eclipse conditions (when the batteries were used). Degradation of the solar arrays occurred much more rapidly than had been predicted for the nominal geostationary orbit. During the early months of the mission, the available solar array power was expected to lead to a constraint on the overall mission duration. Modelling of the radiation damage, and predicting power margins and operational contingency procedures during extended eclipses, was therefore an important part of the operational procedure. This led to improved modelling of the degradation mechanisms, and good prediction of the available power during the later part of the mission.

11.1. Introduction

The power system comprised a solar array, associated sequential switching shunt regulator and battery discharge regulators which regulated the main bus potential to 50 ± 1 V in both sunlight and eclipse periods. Recharge of the power system batteries was achieved by allocating specific solar array cell strings or sections to this particular function.

The solar array consisted of three lightweight panels 120° apart. The panels were very similar to those used on most of the ESA communication spacecraft such as ECS and MARECS. These panels embodied six electrical sections of 142 series connected cells by 7 parallel cells for powering the main bus. A separate battery charge array was composed of six independent cell strings of 126 series connected cells which could be used for either sequential or parallel recharge of the two 28 cell 10 Ah nickel cadmium batteries of the system.

The solar cells were arranged to form main and charge sections. The solar array was based on proven solar generator design concepts, but with some important improvements, including the use of materials such as aluminium honeycomb, together with carbon-fibre reinforced plastic. This gave a lightweight, but highly-loadable structure. Some redesign on the hinge configuration was performed to minimise shock loads created during the latch up of a deploying panel at high satellite spin rates. Each panel was equipped with two hold-down units and one pyro-actuated cable cutter as a release unit.

For the electrical layout, the goal was to design a highly failure-resistant cell design. The solar generator design involved single stringing in all main sections, with individual blocking diodes to limit the effect of power loss in case of a short circuit, as well as an extra thick kapton insulation layer to give a high degree of protection against short circuits. Protection against adverse effects of shadowing of the inner parts of the solar array wings due to attitude control subsystem failure was achieved by incorporating shunt diodes for cell protection.

The protection against electrostatic discharge, which had caused many problems in the past, was designed with great care. To prevent charging of non-conductive structural parts of the front side of the panel, all areas not covered with solar cells were protected with an aluminised kapton foil, which was grounded to the structure of the solar array. The complete rear side, as well as the so-called 'edge members', were painted with conductive black paint. All panel wiring was carefully routed through the edge members and on the panel's rear side, wherever possible.

Mechanical Properties

Each of the three solar arrays was based on a lightweight structure built of aluminium honeycomb and carbon-fibre reinforced plastic: with kapton foil to electrically insulate the cell area from the array structure; special hinges to decrease latch-up shock loads during deployment at high spin rates (up to 10 rpm); and two hold-down points, with pyrotechnic cable cutter release mechanisms. Each of the arrays was 1690 mm long, 1190 mm wide, and 23 mm high. All three panels together weighed about 31 kg.

Electrical Properties

Each of the three solar arrays had two main sections, made up of seven strings with 142 serial connected cells (each string was equipped with a blocking and shunt diode), and two charge sections, each with 126 serial connected cells and shunt diodes to protect against shadowing effects. The cells were back-surface-reflecting high-efficiency units with a thickness of 180 μm. Electrostatic discharge protection was provided by means of grounded aluminised kapton on the panel's front side and conductive black paint on the rear and on edge members. An integrated thermocouple provided subsystem temperature data during the mission, and array deployment and successful latch-up was monitored by separate switches for each panel.

One of the consequences of the satellite being in a geostationary transfer orbit was that the efficiency of its solar panels was degraded by the repeated radiation exposure at a much higher rate than if the satellite had been in geostationary orbit. The consequence of this process led to a potentially shorter lifetime for the mission.

To estimate the lifetime of the satellite, periodic measurements were obtained from the open circuit voltage of the charge array strings. The first results from these calculations resulted in a very pessimistic forecast for the mission. The degradation was considered to be very high and a potential lifetime of only about 6 months was predicted. However, after first collection of real spacecraft data the degradation proved to be far less than the originally predicted values.

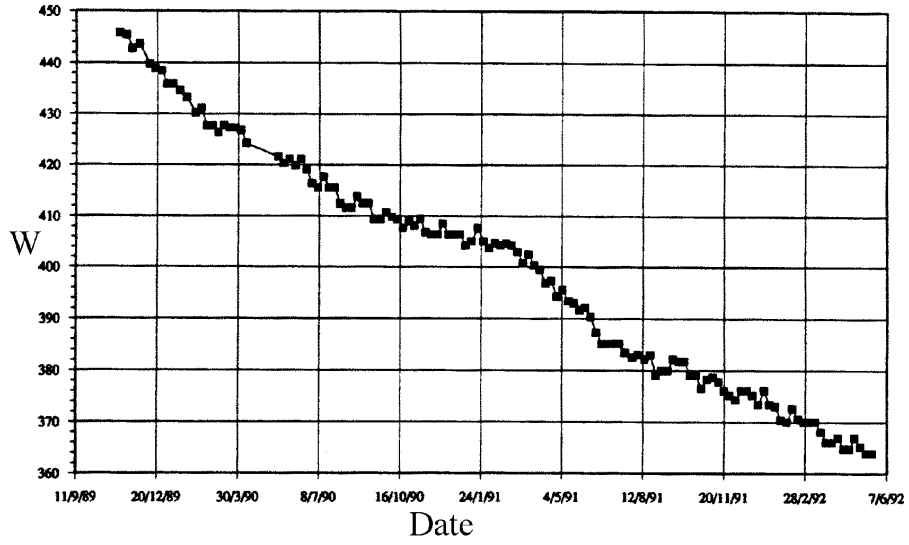

Figure 11.1. *Power provided by the solar arrays as a function of time. The decrease was predicted qualitatively and modelled accurately, as a consequence of radiation damage, as described in Section 11.3.*

11.2. Power Subsystem Degradation

The power supplied by the solar array is shown in Figure 11.1. The power drop from the beginning of the mission to June 1992 was 18 per cent of the initial value. The spacecraft required approximately 270 W in geostationary transfer orbit. Four out of six main sections were activated during the early stages of the mission.

The behaviour of the batteries remained nominal throughout the mission. The planned geostationary orbit would only have required battery operation during much shorter eclipses than those demanded in the case of the actual geostationary transfer orbit. Consequently they had not been designed with these cases in mind. The major constraints to the batteries efficiency under these circumstances were the long eclipse durations associated with a short sunlight time for charging, itself related to the battery power budget (during long eclipses, the satellite could only function by drawing power from the batteries) and the high battery charge/discharge cycle repetition rate.

The evolution of the maximum power margin provided by the batteries was monitored from the start of the mission. The maximum power margin is the difference between the maximum power that the batteries are able to supply during an eclipse, and the usual power consumption of the spacecraft during an eclipse, and is given by $P_{\text{max–margin}} = P_{\text{max}} - P_{\text{sat}}$ with $P_{\text{sat}} = 224$ W. P_{max} calculations took into account the charging current, the maximum charging time, the depth of discharge limit of 65 per cent, and the maximum power the battery discharge regulator could provide (440 W). For $P_{\text{max–margin}}$, P_{max} is the minimum value of 440 W, $P_{1\text{max}}$, $P_{2\text{max}}$, where:

$$P_{1\text{max}} = V_{\text{bat}} I_{\text{ch}} \frac{\eta_{\text{BDR}}}{HK} \frac{T_{\text{ch}}}{T_{\text{ecl}}} \qquad [11.1]$$

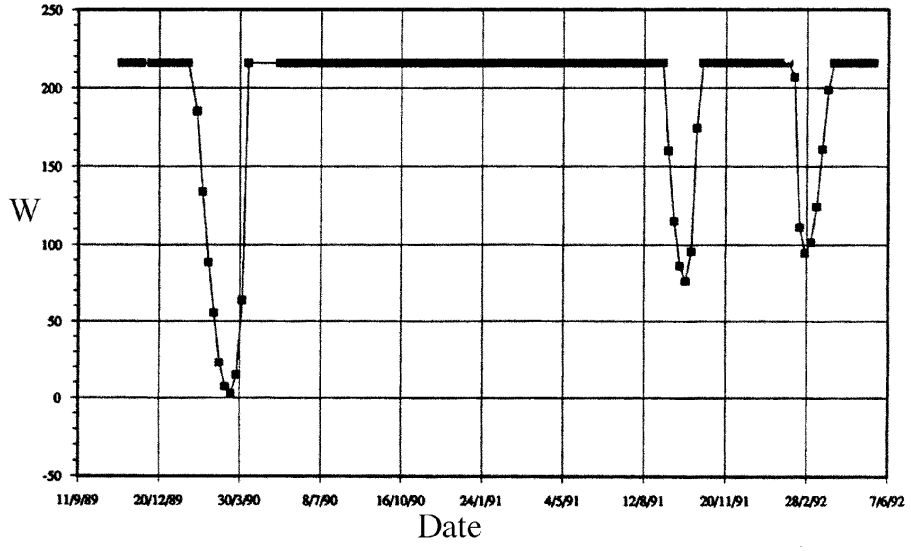

Figure 11.2. *Maximum power margin. The drops in the power margin correspond to the occurrence of the longest eclipse periods; shorter eclipses at other times had no effect on the power margin.*

$$P_{2\max} = V_{\text{bat}} \text{DOD} \frac{\eta_{\text{BDR}}}{H} (2 - 0.082) \frac{N}{T_{\text{ecl}}} \qquad [11.2]$$

V_{bat} is the battery voltage during eclipse = 37.5 V; T_{ch} is the charging time = 10.67–T_{ecl} hours; T_{ecl} is the eclipse duration in hours; H are harness losses = 1.01; K is the charge efficiency = 1.05; DOD is the depth of discharge = 0.65; I_{ch} is the charge current; N the battery nameplate capacity = 10 Ah; and 2 – 0.082 signifies the worst case of battery discharge regulator mismatch of 8.2 per cent. The charging current was directly calculated from the monitored short-circuit current, I_{sc}, which was a function of the solar array degradation and of the seasonal effects.

Prior to the March 1990 eclipse, simulations had indicated that power saving on board the spacecraft would be required to get through the long eclipses. Figure 11.2 shows that the three periods of longest eclipse were passed successfully without power saving. During the longest eclipse (up to 104 min) which occured on 19 March 1990, the margin decreased to 3 W, and the associated depth of discharge reached 60 per cent (Figure 11.3), although the specification limit of 65 per cent was never reached.

A similar study was performed with a linear extrapolation of I_{sc} degradation, and calculated eclipse durations, in order to assess the power margin during the following eclipses of April 1993 and September 1993. The results are shown in Figure 11.4. The batteries were expected to withstand both peaks without power saving on board the spacecraft, although with a power margin falling to about 9 W.

In its actual orbit the batteries underwent approximately 2000 charge/discharge cycles for the three-year mission compared to 125 charge/discharge cycles that had been anticipated in geostationary orbit. Since 25 000 cycles had been obtained in low-Earth orbit tests at 40 per cent depth of discharge over a three-year period at 5° and 25 °C, the charge/discharge factor was not a limiting factor in the satellite operations.

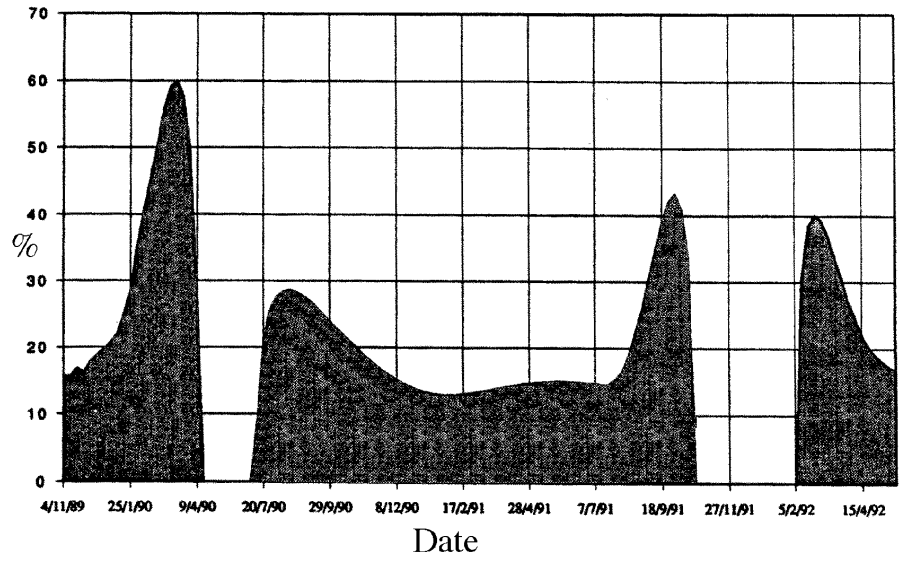

Figure 11.3. *Depth of discharge of the batteries, corresponding directly to the eclipse duration (see Figure 4.1). The maximum specified depth of discharge was 65 per cent. During the longest eclipse period in this interval (19 March 1990) the depth of discharge reached 60 per cent.*

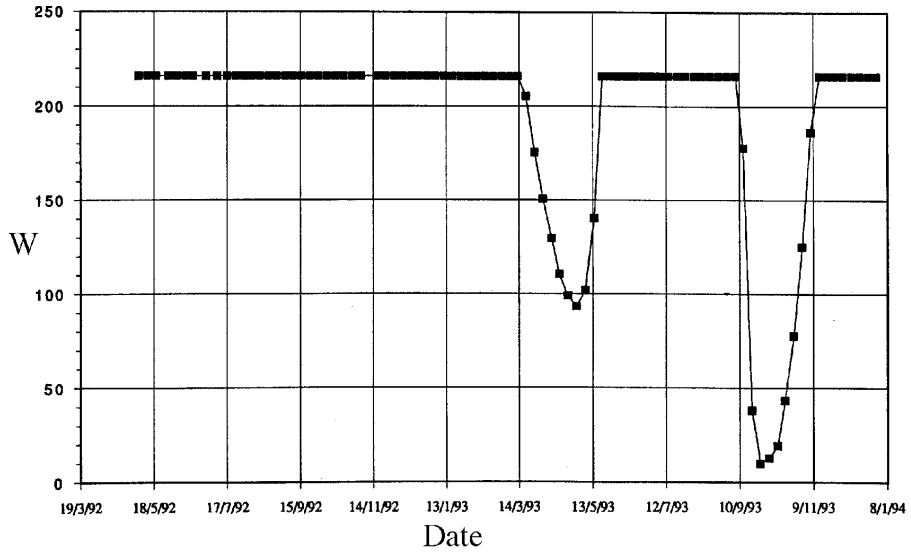

Figure 11.4. *Margin prediction for the future eclipses of April 1993 and September 1993. The first eclipse was passed without power saving (as predicted). Satellite operations terminated in August 1993, before the occurrence of the deeper eclipse.*

11.3. Solar Array Degradation

This section reviews the in-flight and predicted performance degradation of the spacecraft's solar array after three and half years in the very damaging radiation environment of its geostationary transfer orbit. The radiation environment provided a unique opportunity to study the on-board silicon solar cells up to equivalent 1 MeV electron fluence levels of $\phi = 1.26 \times 10^{16}$ e^- cm^{-2} for the short circuit current, I_{sc}, and 2×10^{16} e^- cm^{-2} for P_{max}/V_{oc}, the maximum power to open circuit voltage ratio, seldom attained by other spacecraft.

Radiation Model

Due to its geostationary transfer orbit (inclination 7°, perigee 651 km, apogee 35 835 km and period 10.68 hours) the satellite traversed the complete cross-section of the Earth's van Allen radiation belts. For the purpose of analysis, it was considered to have received intense one hour proton bombardment four times per day. This is depicted in Figure 7.2 which shows the daily positional proton flux encountered.

Although the computer routines used to assess the effects of the radiation environment embodied electron and solar flare components, these were insignificant compared to the proton contribution component of the 1 MeV 'equivalent' electron fluence aggregate. As an example, the daily trapped electron component only amounts to a fluence of 1.4×10^{11} 'equivalent' 1 MeV e^- cm^{-2} compared to 1.2×10^{13} e^- cm^{-2} for the daily proton component. Solar flares were also neglected since their annual contribution only amounts to the trapped proton daily fluence. This 1 MeV equivalent electron irradiation concept (Anspaugh 1991; Tada *et al.*, 1982; Anspaugh & Downing 1984) reduces both electron and proton irradiation effects over a wide energy range down to a single, convenient 1 MeV electron test energy and holds good so long as the electron and proton degradation characteristics take the same qualitative form (Figure 11.5 and Figure 11.6).

Laboratory Experiments

A series of laboratory experiments were carried out to investigate solar cell response to 1 MeV electron and 10 MeV proton irradiations. The two solar cell types tested were each the most radiation resistant of their class. They were the older generation 10 Ω cm silicon cell (Hipparcos type) and the more recent gallium arsenide/germanium (GaAs/Ge) cell; the latest advanced III-V compound cell to enter production. The silicon cells were manufactured by Telefunken System Technik (D) and the GaAs/Ge cells by Applied Solar Energy Corporation (USA).

More specifically the silicon cells were n-p 10 Ω cm, CZ silicon, measuring 2×4 cm^2 and 180 μm thick. They comprised a back surface Al reflector (for achieving lower operating temperature and hence more power output), a TiO anti-reflection coating and TiPdAg weldable contacts. Two thirds of the cells tested (75) were also fitted with nominal 150 μm thick cerium stabilised CMX cover glasses using DC93500 silicon adhesive. The average power output of these cells was 17.13 mW cm^{-2} (η = 12.7 per cent, 25 °C)

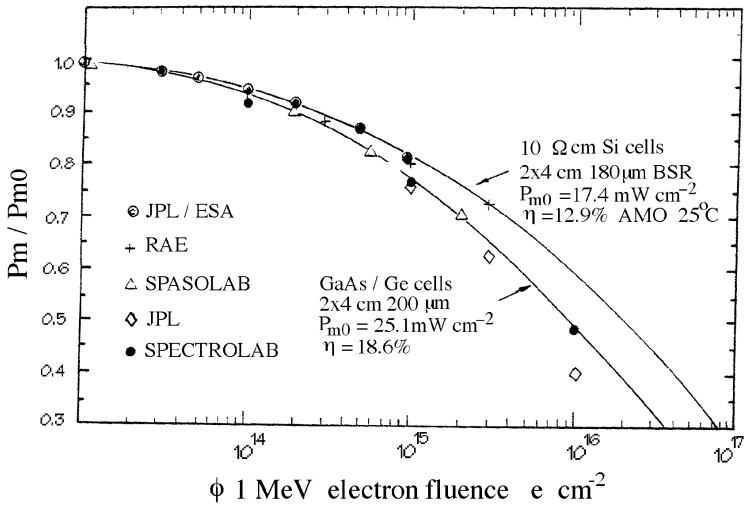

Figure 11.5. *Power loss versus 1 MeV electron fluence for Si and GaAs/Ge solar cells. The ordinate gives the ratio between the power at a given time (Pm), and the power originally provided by the solar arrays (Pm0). The abscissa refers to the equivalent electron fluence, discussed in Chapter 7. The upper curve gives the experimental results obtained for the Hipparcos (Si) cells, while the lower curve shows the degradation applicable to GaAs/Ge cells—although the latter degradation appears to be more significant, the equivalent 1 MeV electron fluence corresponding to a given proton flux is much lower for GaAs/Ge (see Figure 7.7).*

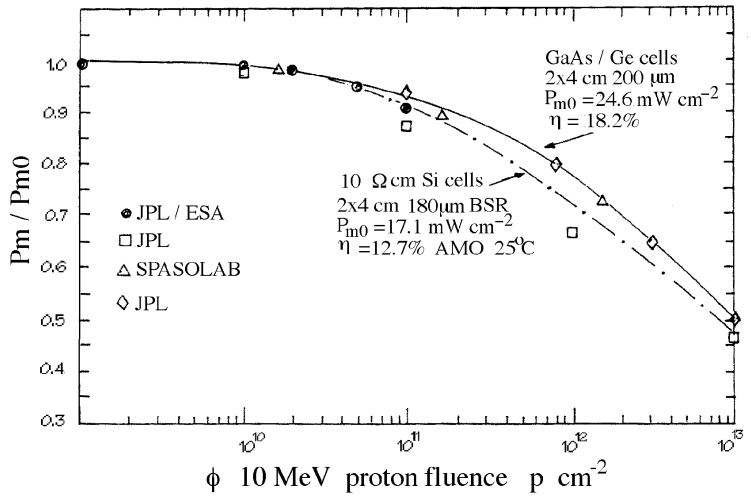

Figure 11.6. *Power loss versus 10 MeV proton fluence for Si and GaAs/Ge solar cells. Details are as for Figure 11.5.*

i.e. 170 W m^{-2}. The average uncovered cell weight was 439 mg yielding a power-to-weight ratio of 38.7 W kg^{-1} for the basic cell.

Six separate CMX cerium stabilised cover glasses were also supplied by Pilkington Space Technology (UK) for testing to facilitate differentiation of radiation-induced optical darkening from basic cell degradation.

The GaAs/Ge cells tested (60) were p-n, metal organic chemical vapour deposition cells (Cheng *et al.*, 1991) measuring 2×4 cm^2 and 200 μm thick. The GaAs to Ge interface was inactive. Half of the cells were covered with 50 μm thick cerium stabilised CMX cover glasses. The average power output of the cells was 24.60 mW cm^{-2} (η = 18.3 per cent, 25 °C) i.e. 246 W m^{-2}. The average uncovered cell weight was 886.9 mg yielding a power-to-weight ratio of 27.7 W kg^{-1} for the basic cell.

Solar Cell Performance Measurements

Solar cell I–V performance measurements were made using reliable pulsed or continuous xenon solar simulators as a light source. A primary standard cell of similar spectral response to that of the test cells was used to set the simulator intensity. The solar cells I–V characteristics were measured with a conventional four-probe measurement system and a power supply for a load. The solar cell temperature was controlled to 25 $\pm$ 0.2 °C during I–V measurements.

1 MeV Electron and 10 MeV Proton Irradiations

The 1 MeV electron irradiations of the covered silicon solar cells were performed using the JPL (USA) Dynamitron accelerator (Anspaugh 1991). The electron beam was spread into a wide uniform beam using an aluminium foil 127 μm thick. Beam intensity is highest at the beam centre and falls off to 91 per cent of the centre value at the edges. The cells were mounted on a copper cell-mounting plate using vacuum grease for good thermal contact. The cell-mounting plate was then bolted onto a fixed target plane in the irradiation chamber. This target plane was temperature controlled to hold the solar cell temperature at 28 °C during the electron irradiations and a Faraday cup was mounted in the centre of this plane for flux and fluence dosimetry. Cumulative fluence exposures were 1×10^{13}, 2×10^{13}, 5×10^{13}, 1×10^{13}, 2×10^{13}, 5×10^{13} and 1×10^{15} e^- cm^{-2}. All irradiations were carried out in vacuum at a pressure below 5×10^{-5} torr.

RAE (UK) subsequently repeated these tests on the uncovered Hipparcos Si cells using a water-cooled vacuum cell holder at their BICC van de Graaff accelerator in London. The 1 MeV electron fluence was extended to 3×10^{15} e^- cm^{-2}.

Spasolab irradiated their assignment of GaAs/Ge solar cells up to a 1 MeV electron fluence of 2×10^{15} e^- cm^{-2} using the University of Delft (NL) van de Graaff accelerator. This facility was also used to irradiate the covered silicon cells together with the individual CMX cover glasses up to very high fluences (3×10^{16} e^- cm^{-2}) to evaluate the radiation 'hardness' of the glasses and their adhesive (DC93500). This particular experiment was repeated, with the inclusion of directly glassed (electrostatically bonded with no adhesive) control cells, on account of the physical effects observed.

The 10 MeV proton irradiations were performed using Tandem van de Graaff accelerators (Anspaugh 1991; Anspaugh & Downing 1984). Beam energy was controlled

by 90° magnetic analysis and the accelerator energy was stabilised by a slit-feedback system to control the van de Graaff terminal voltage. All irradiations and dosimetry were performed in vacuum (less than 5×10^{-6} torr). The small focused proton beam produced by the accelerator was spread into a wide area uniform beam by means of scattering foils. The target plane was approximately 3 m from the scattering foils. The foils were chosen so that the beam intensity at the edge of a 10 cm diameter circle in the target plane varied no more than 7 per cent from the beam intensity at the centre.

The solar cell target plane was rotated at a rotation rate $d\Theta/dt$ proportional to $1/\sin\Theta$, thereby providing a good simulation of the omni-directional space radiation environment by rotation about only one axis. Fluence levels up to 1×10^{11} protons cm^{-2} were studied by JPL for the covered Si Hipparcos cells. Spasolab irradiated their GaAs/Ge cell assignment up to a 10 MeV fluence of 1.59×10^{12} protons cm^{-2} using the CEA accelerator near Paris.

The I–V characteristics of the irradiated cells were measured following 'cool-down' and performance stabilisation by photon irradiation (i.e. under simulated illumination at 25 °C for 48 hours).

In-Orbit Hipparcos Solar Cell Data

The most fundamental indication of the radiation influence was initially obtained from telemetry data of the open circuit voltage (V_{oc}, Figure 11.7) of the charge array strings. A further indication of the radiation environment effect was also regularly obtained from telemetry data of the short circuit current (I_{sc}, Figure 11.8) of one of the main solar array sections, this section being permanently dumped at launch as a result of lower on-board power consumptions than originally anticipated for the mission.

The I_{sc} and V_{oc} data were transmitted from ESOC on a regular basis after normalisation of the data to a solar aspect angle of 0°, air-mass-zero illumination and a cell temperature of 25 °C. The data was also correlated with solar intensity to account for the cyclic variation of the Earth-Sun distance. After February 1990, only solar arrays 1 and 2 were taken into account, since solar array 3 had suffered a thermistance failure. The nominal Hipparcos operating mode was with a solar aspect angle of 43° and a cell temperature of 33°. This was backed up by a 'safe mode' configuration with a solar aspect angle of 0° and a cell temperature of 55 °C. The flight data is probably accurate to ±2 per cent.

The final I_{sc} values result from the satellite sun-pointing mode during the final fifteen days. The operational voltage limit was taken to be 53 V which corresponded to a nominal voltage of 51 V, together with the voltage drop, the blocking diode and the charged quad. The average degradation was about 3 V per year, and extrapolation of the curve shown in Figure 11.8 indicated a lifetime up to the middle of 1994. However, since there was a direct correlation between the degradation of the solar generator and the solar particle flux (particularly the proton flux), the lifetime could be reduced in the event of stronger than predicted solar activity.

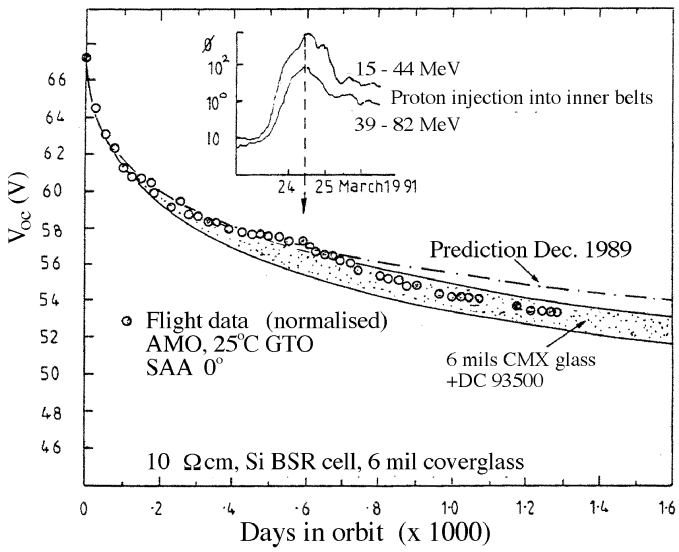

Figure 11.7. *Hipparcos in-flight solar array open circuit voltage (V_{oc}) degradation, normalised to 25 °C, 0° sun aspect angle (SAA), and air-mass-zero illumination (AMO). The dashed line indicates the degradation predicted early in the revised mission (in December 1989). The data points (open circles) correspond to the measured data. The shaded region corresponds to the final predicted performance described in the text, the uncertainty region corresponding to the tolerance on the cover glass thickness (nominally 6 mil; or 0.006 inches). The observed degradation corresponded fairly well with the final assessment of the cell performance.*

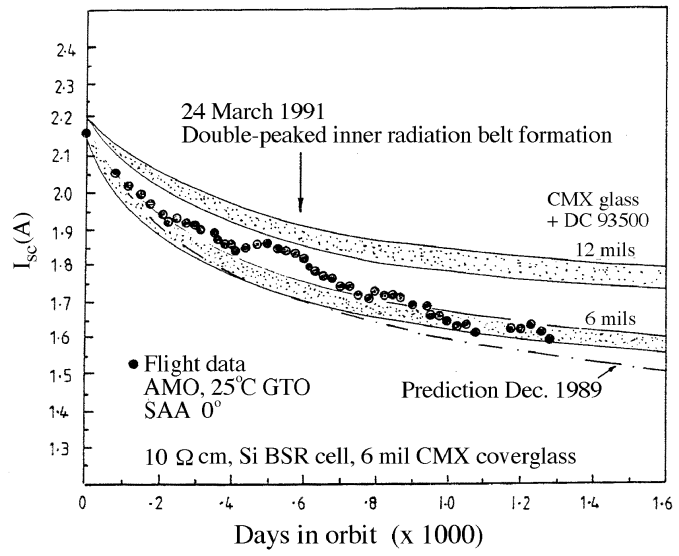

Figure 11.8. *Hipparcos in-flight solar array short circuit current (I_{sc}) degradation. Details are as for Figure 11.7. The observed degradation (solid circles) was less severe than the original (December 1989) prediction. The lower shaded region corresponds to the final model for the actual (6 mil thick) cover glass used for the Hipparcos solar arrays. The upper shaded region indicates the improvement in performance expected had 12 mil thick cover glass (used for GEOS) been used.*

Comparison of Results and Analysis

The results of the 1 MeV electron and 10 MeV proton irradiation experiments are depicted in Figure 11.5 and Figure 11.6 respectively. Additional data points were added from reliable reference sources to enhance the extrapolation of the degradation curves which were needed for making the in-orbit predictions. The partition of Si and GaAs/Ge cell data is distinct for both electron and proton irradiations and the data points from the various experimenters appear to be both complementary and in good agreement with each other. Considering the electron and proton fluence required to produce a 25 per cent loss of maximum cell power output ($P_m/P_{m0} = 0.750$), it is seen that in the case of the GaAs/Ge cells this is achieved for $\phi_1 = 1.3 \times 10^{15}$ e^- cm^{-2} and $\phi_2 = 1.3 \times 10^{12}$ protons cm^{-2} respectively. Thus the ratio $\phi_1/\phi_2 = 2.1 \times 10^{15}/7.5 \times 10^{11} = 2.80 \times 10^3$ e^-/proton, i.e. 2800 1 MeV electrons per 10 MeV proton. This data is consistent with the damage coefficients embodied in the NASA EQFRUX computer routine for silicon cells (Tada *et al.*, 1982) and the latest version applicable to GaAs/Ge solar cells (Anspaugh 1991). The character of these electron/proton ratios is depicted in Figure 11.9 as a function of proton energy and illustrates the proton energy cut-off levels achieved by using various cover glass shielding thicknesses.

Because of the non-uniform nature of the damage produced by low energy protons within the body of a cell, a similar data set had to be derived for short circuit current (I_{sc}) predictions (Tada *et al.*, 1982), i.e. the damage coefficients were partitioned as I_{sc} and P_{max}/V_{oc}.

By using the proton/electron belt radiation maps AP8 MAX and AE8 MAX in combination with the limited laboratory data available and appropriate EQFRUX computer routines, it was possible in December 1989 to make a prediction for the likely course of the Hipparcos solar array short circuit current and open circuit voltage performance degradation for the ensuing years.

These predicted degradation curves are shown in Figure 11.7 and Figure 11.8 for which it had been possible to include the observed flight data and additional refinements to the original predictions based on the latest available experimental data. The original predictions were reasonable; slightly pessimistic in one case and optimistic in the other. The updated prediction curves benefited from more recent laboratory data and higher particle fluences but another factor emerged to introduce another aspect of uncertainty; namely the thickness tolerance of the cell cover glasses and intervening optical DC93500 adhesive. Thus a nominal 150 μm CMX cover glass supply could have an allowable thickness variation from 130–170 μm, a 50 μm CMX cover glass 45–60 μm, a 300 μm cover glass 260–340 μm and so on. The extremities of the 'prediction' bands depicted in Figure 11.7 and Figure 11.8 represent the influence of the upper and lower values of the shielding specific mass.

The sudden discontinuity in the flight data on day 590 corresponds to the sudden solar storm commencement (Mullen *et al.*, 1991) and formation of a double peaked inner radiation belt. A similar effect was observed on the High Efficiency Solar Panel Experiment flown on CRRES (Ray *et al.*, 1993) for a period of 14.5 months i.e. from Hipparcos day 351 to 795. The radiation hardening which would have been achieved had 300 μm (12 mil) thick CMX cover glasses been used, is also shown in Figure 11.9.

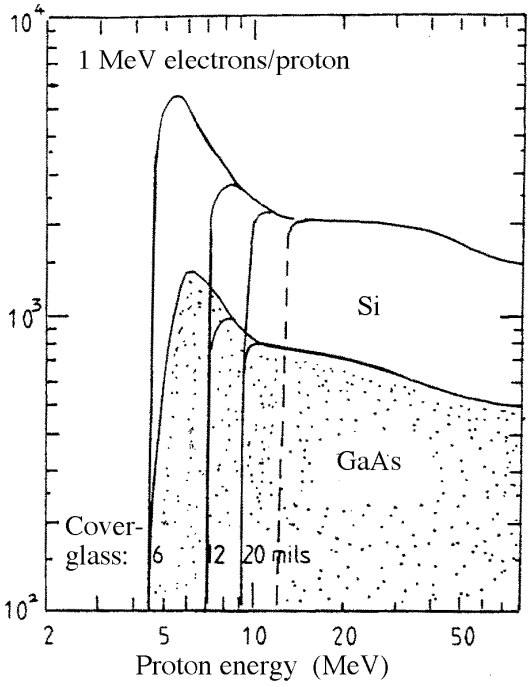

Figure 11.9. *The dependence of the number of equivalent 1 MeV electrons per proton as a function of proton energy, for various cover glass (shielding) thicknesses, and for Si and for GaAs solar cells. The figure illustrates the proton energy cut-off levels achieved by using various cover glass thicknesses. The Hipparcos cells corresponded to the 6 mil (0.006 inch ~ 150 μm) cover glasses on Si.*

Since the Hipparcos solar cell's operating point was now beyond the knee of its I–V curve it was possible to reconstitute its I–V characteristic by monitoring the battery recharge current in this region. This is shown in Figure 11.10 along with estimates of the associated 1 MeV equivalent electron fluences for I_{sc} and P_{max}/V_{oc} degradation.

As a consequence of the advanced stage of performance deterioration an interesting phenomenon was observed. The solar array delivered less power when pointed normal to the Sun (a safe mode in the event of gyro problems) than when in its normal operating mode (solar aspect angle = 43°). This arose because pointing at the Sun causes the cell's temperature to rise from 33 to 55 °C thereby lowering V_{oc} still further.

Concerning the durability of the cell's optical components at high fluence 1 MeV electron irradiation (Delft University), at $\phi = 3 \times 10^{16}$ e^- cm^{-2}, it was observed that several cover glasses had started to delaminate. This is shown in Figure 11.11. Subsequent microscopic examination and dissection revealed that advanced polymerisation and hardening of the DC93500 silicone adhesive had taken place and was followed by delamination at the cover glass/adhesive interface. The influence on the electrical performance of the cell was negligible (1 per cent). A repeat experiment was conducted with directly 'glassed' cells (i.e. electrostatically bonded with no adhesive) included as a control. These cells showed no such deterioration but several of the conventionally covered cells again displayed cover glass delamination. The six individual CMX cover glasses were also subjected to this high fluence level but exhibited no measurable deterioration of their transmission characteristics (Figure 11.12.)

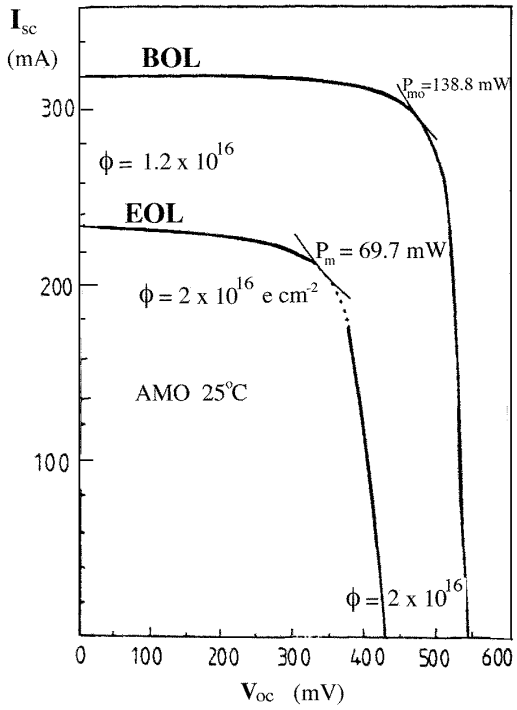

Figure 11.10. *Hipparcos solar cell I–V characteristics; at launch and after 1280 days in geostationary transfer orbit. V_{oc} and I_{sc} were measured for the array, and the figure indicates the estimated corresponding performance of the cell. The values of P_m indicate the maximum power points at the beginning-of-life (BOL) and end-of-life (EOL).*

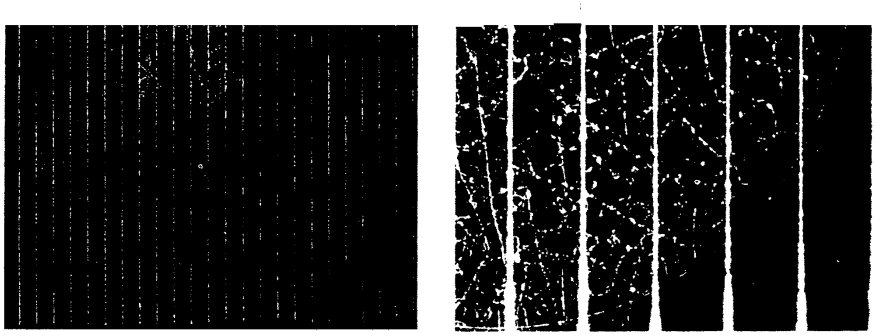

Figure 11.11. *Cover glass adhesive degradation. The vertical white lines are contacts on the solar cell (the separation between two such contacts is approximately 1 mm). The 'crazed' areas indicate delamination in the cover glass adhesive at very high radiation levels, typical of the end-of-life of the Hipparcos mission.*

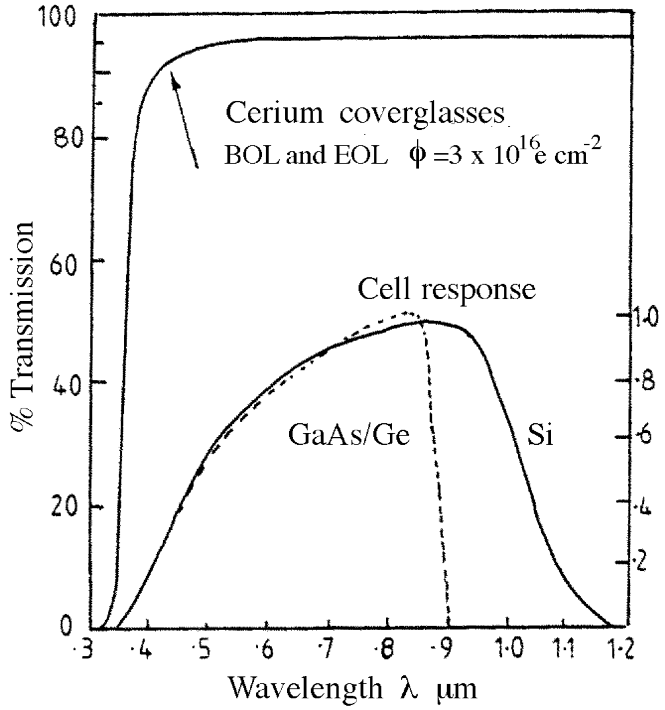

Figure 11.12. *Transmission characteristics of cerium stabilised cover glasses (corresponding to the Hipparcos cells) before and after high fluence 1 MeV electron irradiation. The upper curve is the same at the beginning- and end-of-life (BOL and EOL) indicating the stability of the cover glass. The lower curves indicate the intrinsic cell response as a function of wavelength—the cover glass is optimised to give the highest transmission over the relevant wavelength region.*

The study was concluded by making EQFRUX computer runs for both the Si and GaAs/Ge solar cells in order to compare their radiation hardness in geostationary transfer orbit for 1311 days as a function of cover glass/adhesive shielding. The resultant solar cell maximum power output curves are presented in Figure 11.13, each band extremity representing the permitted tolerance level for the nominal cover thickness indicated. Both cell types are thus expected to be very radiation resistant degrading at approximately the same rate as each other for a given cover shielding and with a marked fall off in hardness in both cases for cover glasses thinner than 150 μm. This is a direct consequence of the high non-linear rise in damage coefficient values at low proton energies (Figure 11.9).

In practice, these predictions were found to be somewhat pessimistic. The CRRES satellite, which operated for 14.5 months in a similar orbit, embodied the same cell types as employed in the present study (Ray *et al.*, 1993). Thus for the case of 300 μm (12 mil) cover glasses thickness the P_{max} of the GaAs/Ge cells degraded by 13 per cent compared to the 16 to 19 per cent predicted by Figure 11.13, while the P_{max} of the Si cells degraded by 16 per cent compared to the 23 to 27 per cent indicated by Figure 11.13. The qualitative 'fan effect' of Figure 11.13 was also confirmed.

In conclusion, the observed in-orbit radiation damage characteristics of the Hipparcos silicon solar cells were predicted reasonably well using proton and electron maps (AP8 and AE8) and NASA computer routines based on the equivalent 1 MeV electron irradiation concept. The accuracy was sufficient to facilitate optimum on-board power system

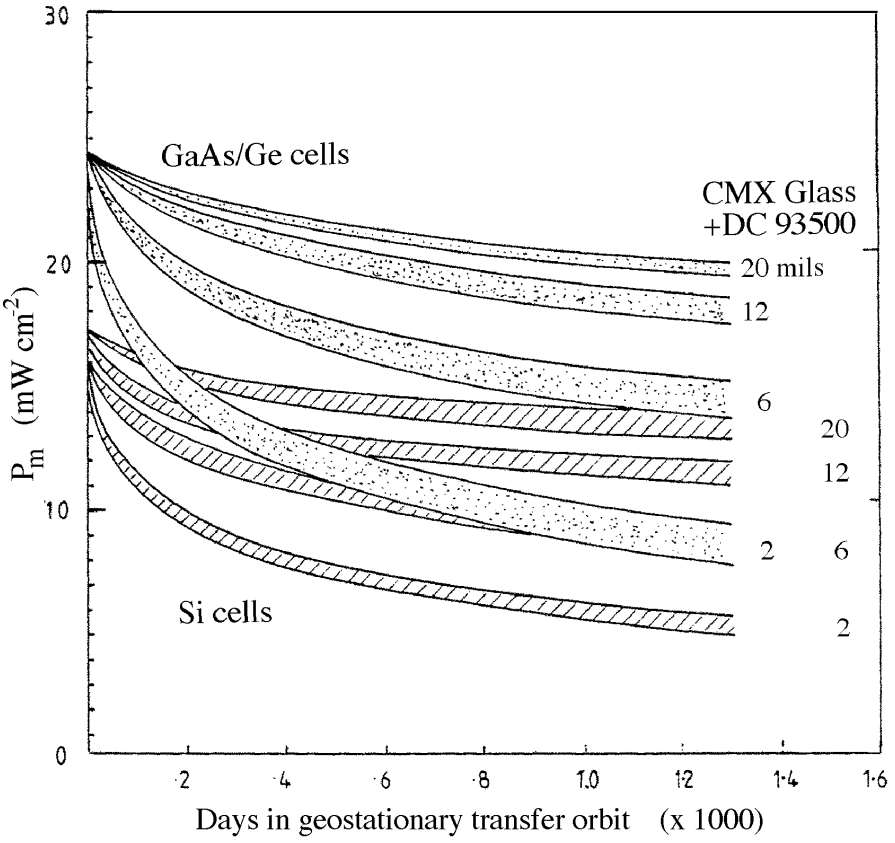

Figure 11.13. *The solar cell maximum power output (P_m) versus time, illustrating the radiation 'hardness' in geostationary transfer orbit for GaAs/Ge and Si arrays (the Hipparcos cells corresponded to the 6 mil (0.006 inch) Si cells, the other configurations being shown for comparison).*

management for the three and half years in geostationary transfer orbit. It was also concluded that the same computational procedure would be suitable for use with the next generation of radiation resistant, high power GaAs/Ge solar cells. Additional laboratory irradiation experiments would, however, be required at high proton/electron fluences and at low, near-shielding cut-off energies, to enhance the accuracy of predictions.

The single most important physical factor influencing the longevity of either cell type in space was found to be the choice of cover glass shielding. The wide range of manufacturing tolerances introduces an uncertainty in the cover glass thickness which must be taken into account. With regard to the durability of the optical cover glass/adhesive components, the use of cerium stabilised cover glass shielding was observed to be appropriate for this application.

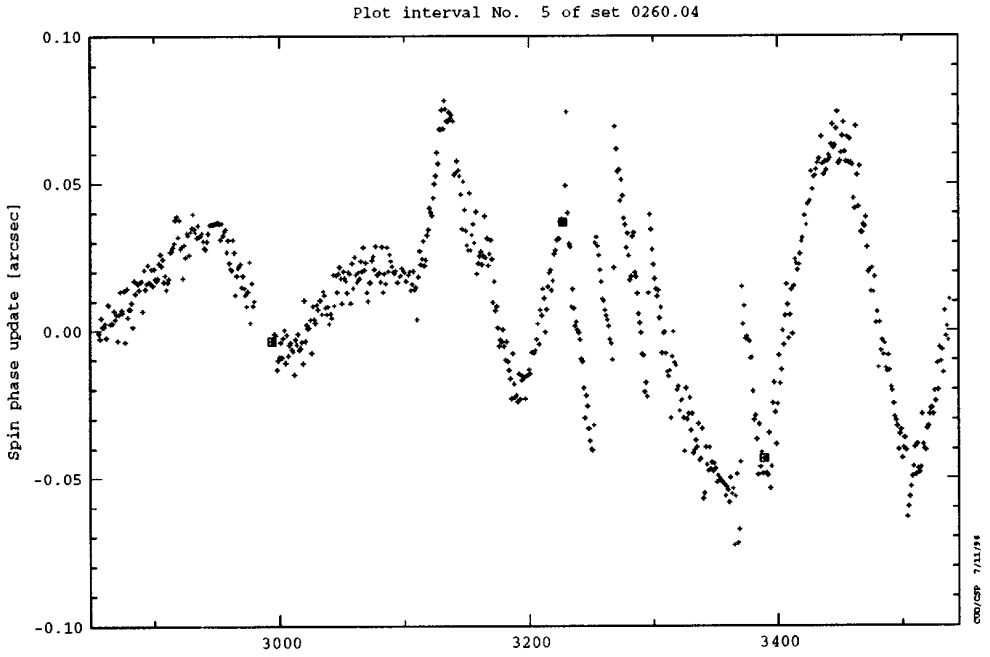

Figure 11.14. *Data interval illustrating the attitude jitter in the along-scan direction occasionally observed after the satellite emerged from eclipse to sunlight. The along-scan attitude is seen to develop smoothly up to frame number 3200, then a series of discontinuities or 'glitches' occur for the subsequent 100 frames (1 frame = 2.133 . . . s); thereafter the attitude develops smoothly again. Squares indicate times of thruster firings.*

11.4. Eclipse-Induced Attitude Jitter

During the on-ground attitude reconstruction, the NDAC Consortium reported intermittent short stretches of data during which the satellite along-scan (spin-phase) attitude updates derived in the great-circle processing showed an unexplained sawtooth behaviour: over some 5 min duration, a series of discontinuities of up to about 50 milliarcsec amplitude, separated by up to approximately 1 min, were observed (see Figure 11.14). The FAST Consortium subsequently confirmed the effect, and threw further light on the problem by noting that the phenomenon occurred some 100 observation frames (roughly 3 min) after the satellite emerged into sunlight after an eclipse period. A single opposite case was noted, less marked, and corresponding to an entry into umbra. It was tentatively proposed that thermal shocks were occurring in the optical structure. It should be noted that the problem affected an almost insignificant fraction of the entire data set, and the affected data were suppressed from the subsequent steps of the data analysis.

The following explanation was eventually formulated, although full confirmation would have required a more detailed study of the solar arrays, their attachment to the satellite, and their thermal environment entering and exiting the eclipses.

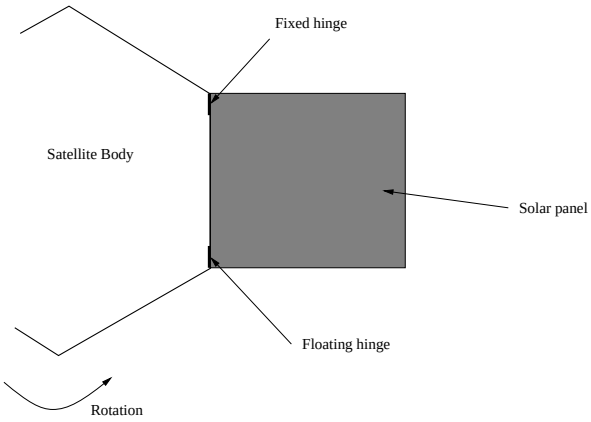

Figure 11.15. *The configuration of one of the solar arrays and its attachment to the body of the satellite. Thermal shocks after eclipses were considered responsible for small discontinuities in the along-scan attitude.*

For each of the three deployable solar panels, one of the hinges was rigidly fixed to the satellite body, while the other allowed some movement along the line of the attachment of the array to the satellite body, this construction allowing for differential expansion between the satellite body and the panels themselves (see Figure 11.15). The solar arrays are held by a carbon-fibre reinforced plastic structure having a very low coefficient of thermal expansion of about 1.5×10^{-6} K^{-1}. For a panel dimension of about 1 m, and a change in solar array temperature of about 100–150 K (the ambient temperatures being about 300 K in sunlit phase, and 170 K in eclipse) a change in dimension of some 0.2 mm (total) would result from passage from umbra to sunlight, and vice versa (the thermal variation of the satellite body was very much smaller because of its larger thermal capacity). It is considered likely that the resulting differential expansion occurred with a 'slip-stick' or 'stiction' behaviour, with the timescales involved (i.e. with the start of the phenomenon occurring 2–4 min after the thermal discontinuity, with an overall duration of a few minutes) well matched to the thermal time constant of the solar arrays provided in the manufacturer's reports.

The sharpness of the transition from umbra to sunlight depended on the satellite position along the orbit, and it was inferred that the effect would be more dramatic for shorter penumbra durations, or less dramatic for shorter total eclipse durations (where the maximum temperature excursion would not be reached). These features were qualitatively confirmed by the data analysis groups.

The transition from shade to sunlight had a more dramatic effect on the satellite motion than that from sunlight to shade. In the former case, with the arrays initially colder, the coefficient of friction between the affected surfaces would be larger than in the latter, and the stiction effect correspondingly larger. At the same time, the lower temperature would result in higher stresses in the hinges or joints (due to thermal contraction) and would thus also increase the friction between the moving surfaces. In summary, it was also considered likely that the effects on entering/exiting eclipse would indeed be 'asymmetrical'.

The magnitude of the phenomenon (50 milliarcsec discontinuities) was consistent with the slip-stick effect of the 10 kg solar array mass located 1 m from the satellite centre

of mass. The following analysis provided an order-of-magnitude estimate of the effect. The impulse of the moving element was estimated from:

$$i = m^* \Delta v \qquad [11.3]$$

where m^* is the solar panel mass. Assuming that the impulse duration corresponds to the fundamental frequency of the solar panel in the relevant plane:

$$\Delta v = 2\pi n^* \Delta u \qquad [11.4]$$

and assuming $n^* = 100$ Hz, $\Delta u = 0.2$ mm, $m^* = 10$ kg, gives $\Delta v = 0.1$ m/s and $i = 1.2$ kg m/s. The assumed n^* was taken as a realistic upper limit for the solar panels, but it could be as low as 10 Hz.

For a satellite moment of inertia of 1000 kg m^2 about the z-axis, the effect on the satellite movement is:

$$a\, i = I\, \Delta\Omega \qquad [11.5]$$

where a is the distance between the mass and the centre of gyration, and:

$$\Delta\theta = \Delta\Omega/(2\pi n) \qquad [11.6]$$

Assuming $n = 100$ Hz for the satellite (this could perhaps be in the range 30 – 200 Hz), and $a = 1$ m gives $\Delta\theta = 1.8 \times 10^{-6}$ rad = 0.4 arcsec.

There are certain complications in applying this simple model: (i) n and (especially) n^* are unknown; (ii) $a\, i$ is an upper limit due to the fact that plane of the panels are offset from the satellite centre of mass (a similar but smaller effect would therefore also be predicted about the other two axes); (iii) the combined effects of the three panels makes the results more complex; (iv) the above calculations led to an oscillatory motion of the given amplitude at the fundamental frequency, not a uni-directional displacement. But, in summary, it did not seem surprising that the effect was observable.

The solar array explanation seems most plausible, given the mass of the panels, rather than any effect of, say, the aluminium fill-in antenna albeit with its larger coefficient of thermal expansion. Effects on the payload itself were also considered to be unrealistic given the known thermal environment.